IMAGE ANALYSIS OF ACOUSTICALLY EXCITED BLUFF BODY FLAMES

An Undergraduate Thesis

by

Dmitriy V Plaks

In Partial Fulfillment
of the Requirements for the Degree
Bachelor of Science in the
School of Aerospace Engineering

_____

Advisor: Dr. Tim Lieuwen

_____

Reader: Dr. Jerry Seitzman

Georgia Institute of Technology
Fall 2007

1. Abstract

This thesis analyzes the effects of various bluff bodies on the downstream flow field. Bluff bodies, for example, those typically found in jet engine augmentors, are objects designed to impede the flow in order to stabilize a flame. The effects of different bluff body shapes (cylindrical and triangular), size (6.35 mm, 9.53 mm, 12.7 mm, and 19.1 mm) and heat release are examined with respect to their influence on downstream vorticity strength, vortex separation distance, and vorticity divergence angle. Particle Image Velocimetry (PIV) is used to obtain the velocity field data from which the vorticity field is calculated. The mean flow velocity, U_∞ is 2.7 m/s, and the flow is acoustically excited at 300 Hz with a normalized acoustic velocity of $u'/U_\infty = 0.8$. The vorticity divergence angle increases with increasing bluff body size, is not affected by bluff body shape, and has a non-linear correlation with heat release. Downstream vorticity strength is affected by all three parameters (bluff body shape, size and heat release) in a non-linear manner. Vortex separation distance is a function primarily of bluff body size, increasing for larger bodies; however, the separation distance decreases with increasing heat release. Bluff body shape also has an effect on vortex separation distance as the cylindrical bluff body creates a larger separation distance between vortices.

2. Acknowledgments

I would like to thank everyone at the Georgia Tech Combustion Lab for their moral support. I would also like to thank Dr. Tim Lieuwen for giving me the opportunity to prove myself. I am particularly grateful to Santosh Shanbhogue for guiding me along my path, educating me, and providing advice about life, the universe and everything.

3. Introduction

The objective of this thesis is to improve understanding of stability of the combustion process in reacting high speed flows. This work is motivated by the problem of combustion instabilities in such devices as jet engine augmentors and duct burners [1]. Typically in these devices the primary instabilities arise due to complicated coupled interactions between the flame oscillations, vorticity fluctuations, and heat-release fluctuations [2].

To stabilize flames in jet engine augmentors, bluff bodies are often used as flame holders. The flow past a bluff body (a body whose cross-sectional area is typically circular or triangular) is defined by three distinct features: a separated shear layer (the interface between two distinct streams), a boundary layer (a layer very near a solid wall where the velocity is lower than that of the general flow), and a wake (the turbulent region immediately downstream of the bluff body) [3]. Two different types of flows are studied: cold flow (i.e., a non-reacting air flow at room temperature) and hot flow (e.g., an exothermic mixture of methane and air with an adiabatic flame temperature ranging from 1750 – 2000 K). Cold flows and hot flows with a temperature ratio between burned and unburned gas $T_b/T_u < 2$ are dominated by two distinct types of instabilities [2,4]. Very near the bluff body the shear layer instability is the main effect, characterized by symmetrical vortex shedding (production of vortices at the trailing edge of the bluff body that move downstream with the flow) [3]. Further downstream the primary instability is the von-Karman instability characterized by antisymmetric vortices (180° out of phase) [3]. In hot flows with $T_b/T_u > 2$, the von-Karman instability is suppressed, and only the shear layer instability is observed [4,5].

To study such instabilities in a safe and repeatable environment, an acoustic excitation source is utilized here. These acoustic excitations produce velocity fluctuations, which in turn, produce shear

layer instabilities and wake mode instabilities. These three effects produce flame position fluctuations that lead to heat release fluctuations [2,6,7]. This interaction process is illustrated in Figure 1. It is thus evident that in order to understand the effects of acoustic excitation one must study the velocity field near the bluff body.

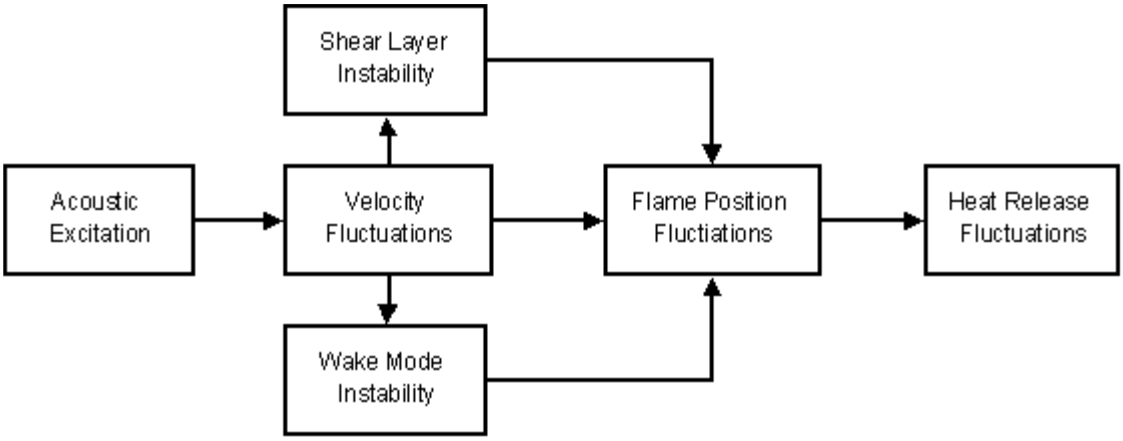

Figure 1: Diagram of how acoustic excitation leads to heat release fluctuations. Acoustic excitations lead to velocity fluctuations which produce instabilities in the shear layer and in the wake. Velocity fluctuations, shear layer instabilities and wake mode instabilities lead to flame position fluctuations, which, in turn, produce heat release fluctuations.

4. Methods

4.1. Experimental Setup

The experiments are conducted at atmospheric conditions in a burner with a square cross-section (3.75” x 3.75”) 3' in length (see Figure 2). Natural gas and air are premixed upstream of the combustor. The flow rates are measured with Dwyer rotameters having ranges of 10-100 SCFM, 25-40 SCFH, and 60-600 SCFH, respectively for air, fuel, and seeding, with accuracies of 2%. After leaving the mixing chamber, the flow travels up into a honeycomb flow straightening section. Just above this section, two 100W Walsch PA acoustic loudspeakers are placed and used to generate acoustic waves.

They are driven by an Agilent 33120A 15 MHz function generator connected to a RadioShack MPA-101 100W amplifier. The flow then travels upward to the burner exit.

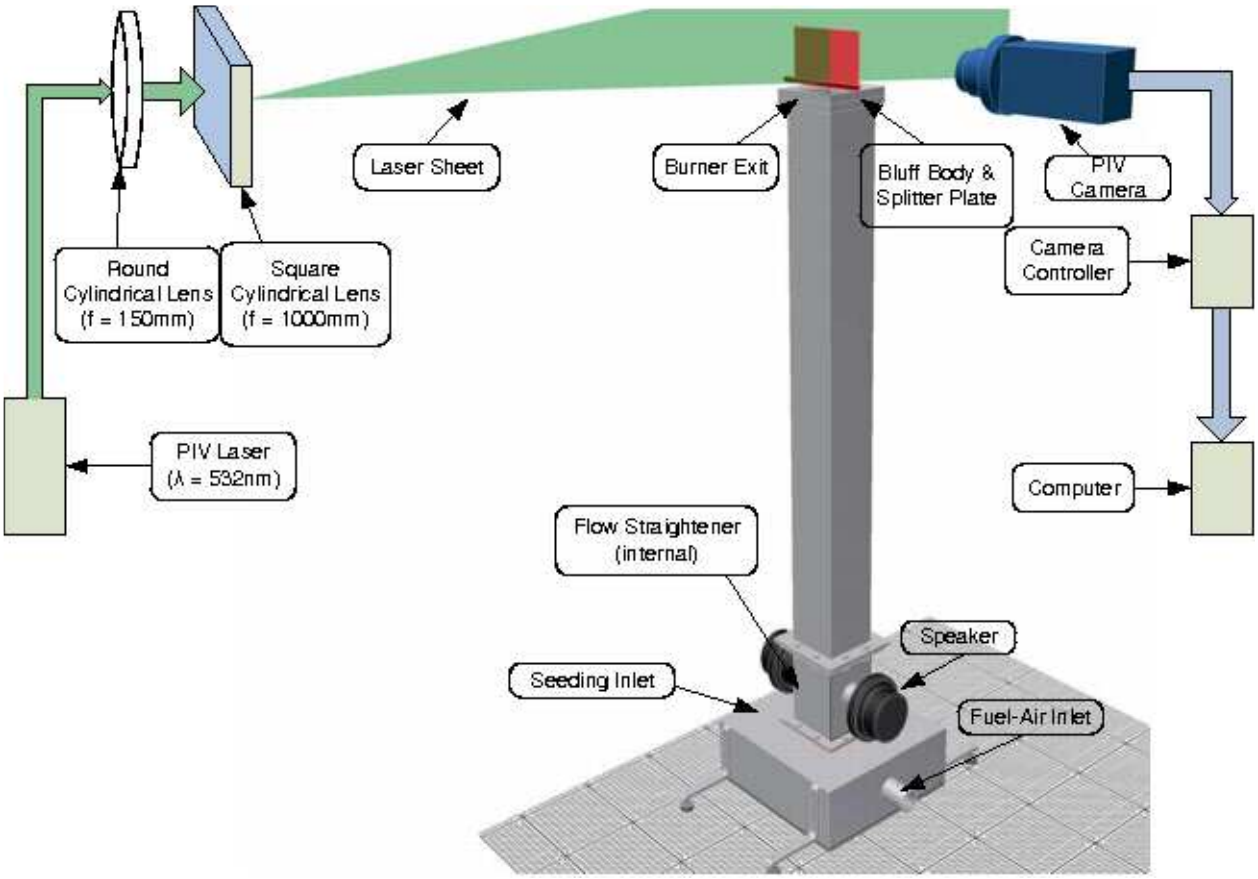

Figure 2: Diagram of Experimental Setup. The flame (not pictured) sits at the burner exit around the bluff body. It is illuminated by the laser sheet and captured by the PIV camera. The premixed flow and seeding particles enter at the base of the burner.

The velocity field is characterized with particle image velocimetry (PIV) [8]. The light source used is a dual head Nd:YAG laser of wavelength 532 nm with a peak power output of 120 mJ/pulse. The interval between the beam pulses is set to 30 μs. The light sheet is generated using two cylindrical lenses of 150 mm and 1000 mm focal length. The lenses are used to reduce the thickness of the 5 mm laser beam and expand it to a height of 40 mm. A 1600x1200 pixel CCD camera, with an F-mount

Nikon 55mm micro-lens with an aperture of f/5.6, is used for imaging. The distance between the imaging plane and the camera is set at 12 inches.

Phase synchronization of the excitation signal with the PIV system is managed by a LaVision timing generator. Images are acquired at an approximate rate of 15 Hz. This is much lower than the excitation frequency, and thus a true time series evolution is not possible. At each phase, 128 images are recorded, and the resulting data is ensemble averaged to provide data (velocity and vorticity) repeatable to within 2% of the reported average value.

The velocity vectors are processed from the raw seeding images using DaVis 7.0 commercial software. The field of view (37 mm x 28 mm) is split into interrogation regions of 64 x 64 pixels, with a 50% overlap. This combination yields a spatial resolution of 1.5mm.

Experiments are performed at an approach velocity U_∞ = 2.7 m/s and excitation frequency f=300 Hz (unless otherwise noted). The amplitude of acoustic excitation, measured at the exit plane of the burner with the bluff body removed, is kept constant at u'/U_∞ = 0.8, where u' is the acoustic amplitude such that the total velocity is

$$u(t) = U_\infty + u' \sin(ft) \tag{1}$$

4.2. Mathematical Methods

The PIV system produces velocity data. This data by itself is very interesting; however, the focus of this study is vorticity. For a general case, vorticity ($\vec{\omega}$) is defined as

$$\vec{\omega} = \nabla \times \vec{V} \tag{2}$$

where $\vec{V}$ is the velocity field. For a two dimensional system (i.e., three dimensional flow features are small), the *x* and *y* components of $\vec{\omega}$ become zero resulting in

$$\omega_z = \frac{\partial v}{\partial x} - \frac{\partial u}{\partial y} \tag{3}$$

where *u* and *v* are the *x* and *y* components of velocity, respectively. Using Eq. (3) the vorticity field is calculated for all images.

4.3. Equivalence Ratio Calculation

In many combustion applications, the equivalence ratio is the most important parameter when determining system performance [9], and it is extensively used in this thesis. The equivalence ratio is defined as

$$\varphi = \frac{F / A}{F / A_{stoic}} \tag{4}$$

where *F/A* is the fuel-to-air ratio as measured in the flow, and F/A_{stoic} is the stoichiometric fuel-to-air ratio as calculated from the combustion reaction equation

$$CH_4 + 2\left(O_2 + 3.76N_2\right) \rightarrow CO_2 + 2H_2O + 7.52N_2 \tag{5}$$

where CH_4 is the hydrocarbon composition of pure methane. Natural gas contains methane as the main ingredient but also includes ethane, carbon dioxide, oxygen, and other substances in very small quantities producing an average molecular weight of 16.384 kg/kmol (average molecular weight of methane is 16.043 kg/kmol).

5. Results and Discussion

The utilization of a bluff body is a popular flame stabilization method [10]; however, careful consideration must be given to the shape and size of the bluff body due to its effects on the overall flame and flow field. In this study, five bluff bodies of various shape and size are used (Figure 3).

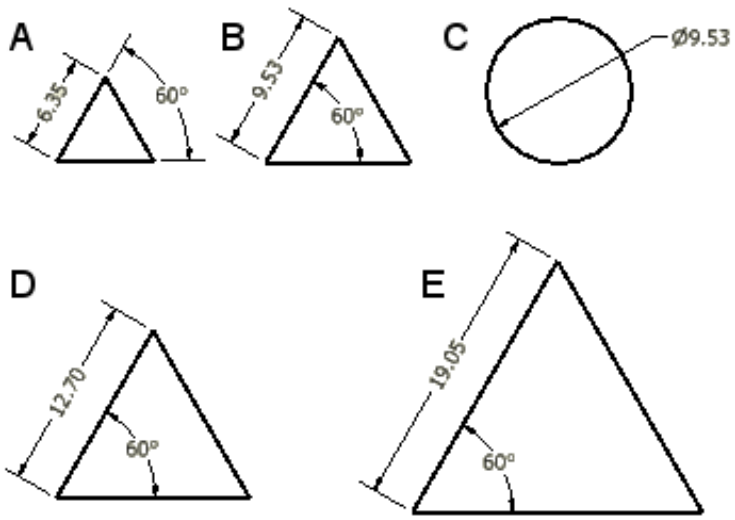

Figure 3: Dimensions of the bluff bodies. Bluff bodies A, B, D and E are equilateral extruded triangles. Bluff body C is an extruded circle (i.e., cylinder). Bluff body B is used to establish a baseline case and all further comparisons are done with reference to body B. All dimensions are in millimeters.

5.1. Effects of Varying Bluff Body Shape

In order to analyze the effects of bluff body shape, the 9.53 mm triangular bluff body and the 9.53 mm circular bluff body (Figure 3 B and C, respectively) are tested. Two cases are studied: unforced case (i.e., no acoustic excitation) and a forced case with 180° phase (with respect to the input acoustic signal). These results are shown in Figure 4 and Figure 5.

The vorticity results shown in Figure 4 lead to several observations for the unforced case. First, no clear vortices are seen because the vortex shedding frequency is independent of the image capture frequency and the images are time averaged. The recorded images capture a random distribution of vortex locations. When these images are averaged together, the resulting plot vaguely resembles an exponential decay in downstream vorticity as opposed to individual vortices (as seen in Figure 5). Second, the vortex strength at the trailing edge of the bluff body (the left edge of the plot) is much stronger in the triangular bluff body case because of the aerodynamic difference between the two bluff bodies. Since the triangular bluff body is less streamlined than the cylindrical bluff body, it produces a much greater recirculation region in the wake. In addition, the flow separation occurs at the trailing edge of the triangular bluff body due to the sharp corner which also contributes to the increased vorticity. Third, the vortex separation distance at the trailing edge of the triangular bluff body is greater than of the cylindrical bluff body (though, this effect is not seen in the acoustically excited case shown in Figure 5).

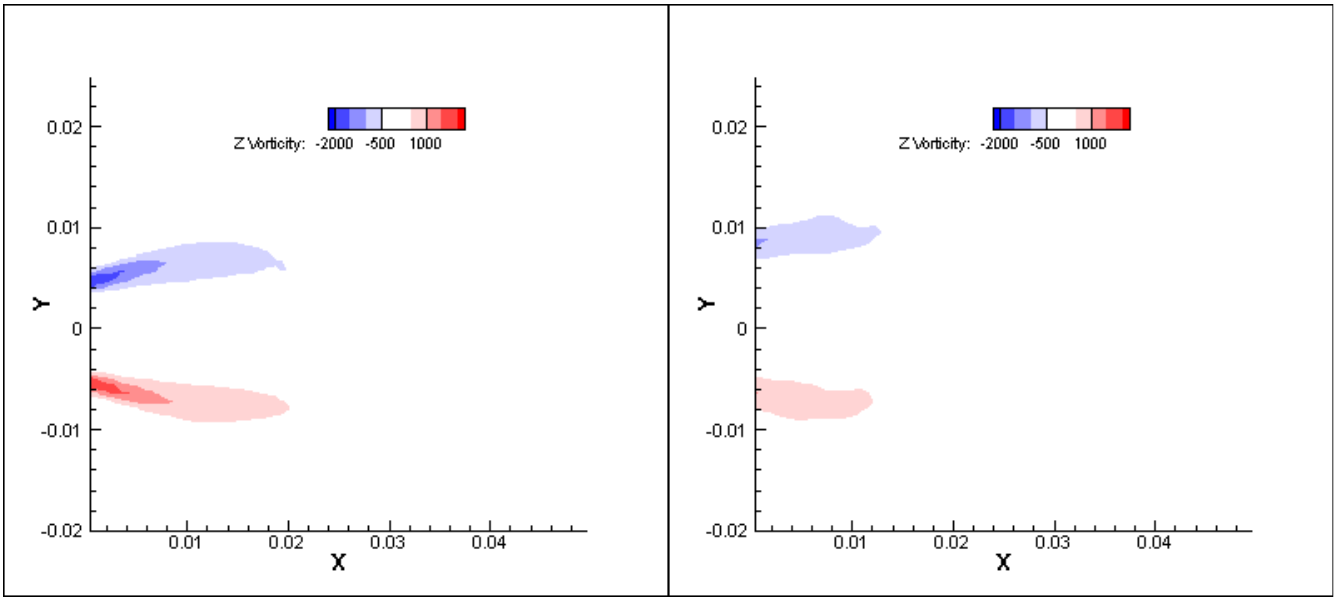

Figure 4: Vorticity plots of the 9.53 mm triangular bluff body (left) and of the 9.53 mm bluff body (right) without acoustic excitation. Axes are in units of meters and the flow direction is from left to right. The bluff body trailing edge is at x = -0.002 m, and the centerline is along the y = 0 line.

Similar effects are seen in the acoustically excited case (Figure 5). The vortices are much stronger at the trailing edge of the triangular bluff body than the cylindrical bluff body. Also, the vorticity field extends further downstream in the triangular bluff body case. In addition to the above mentioned characteristics, the divergence angle is an interesting parameter to consider. For the purposes of this paper, the divergence angle is defined as the angle of the maximum vorticity line (maximum vorticity along the x-axis for each vortex, i.e., one for the top vortex and one for the bottom) to the x-axis. For the case of acoustically excited flow (Figure 5), the divergence angle is defined as the line connecting the vortex centers. Comparing the triangular bluff body to the circular bluff body, there is no apparent difference between divergence angles.

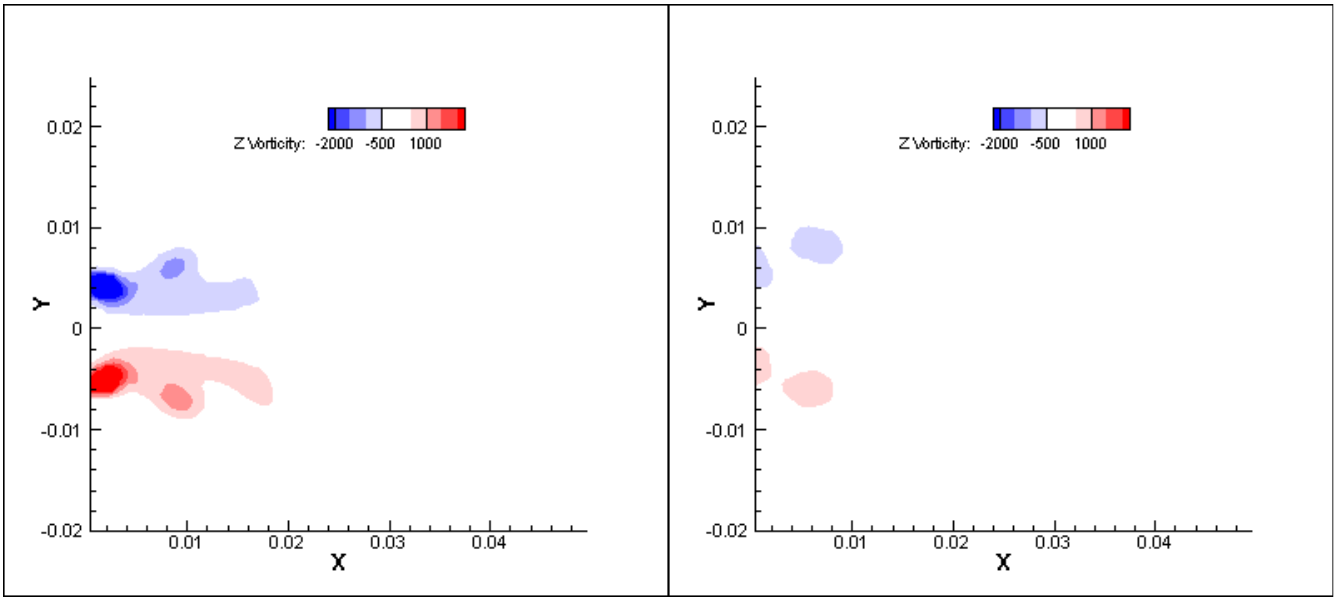

Figure 5: Vorticity plots of the 9.53 mm triangular bluff body (left) and of the 9.53 mm bluff body (right) with acoustic excitation at 300 HZ, 180 degrees phase (with respect to the input acoustic signal) and $u'/U_\infty = 0.8$. *Axes are in units of meters and the flow direction is from left to right. The bluff body trailing edge is at x = -0.002 m, and the centerline is along the y = 0 line.*

5.2. Effects of Varying Bluff Body Size

To study the effects of different bluff body sizes, four triangular bluff bodies are considered: 6.35 mm, 9.53 mm, 12.7 mm and 19.1 mm. Figure 6 shows the vorticity plots for these cases under no acoustic excitation. From this plot, two conclusions arise. First, the divergence angle (as defined in the previous section) increases with bluff body size. Second, the separation distance between the vortex centers increases with bluff body size. This result is rather obvious, since the larger bluff body has a greater separation distance between the top and bottom flow (as viewed in the plots). For larger bluff bodies, this separation distance has no significant impact; however, for the 6.35 mm bluff body (Figure 6 top left and Figure 7 top left), the top and bottom vortices are close enough that they interact and partially negate each other. This effect results in faster downstream vorticity decay. Also, the

downstream vorticity decay is much smaller for the 6.35 mm bluff body (Figure 6 top left), but no conclusive difference is seen between the larger bluff bodies.

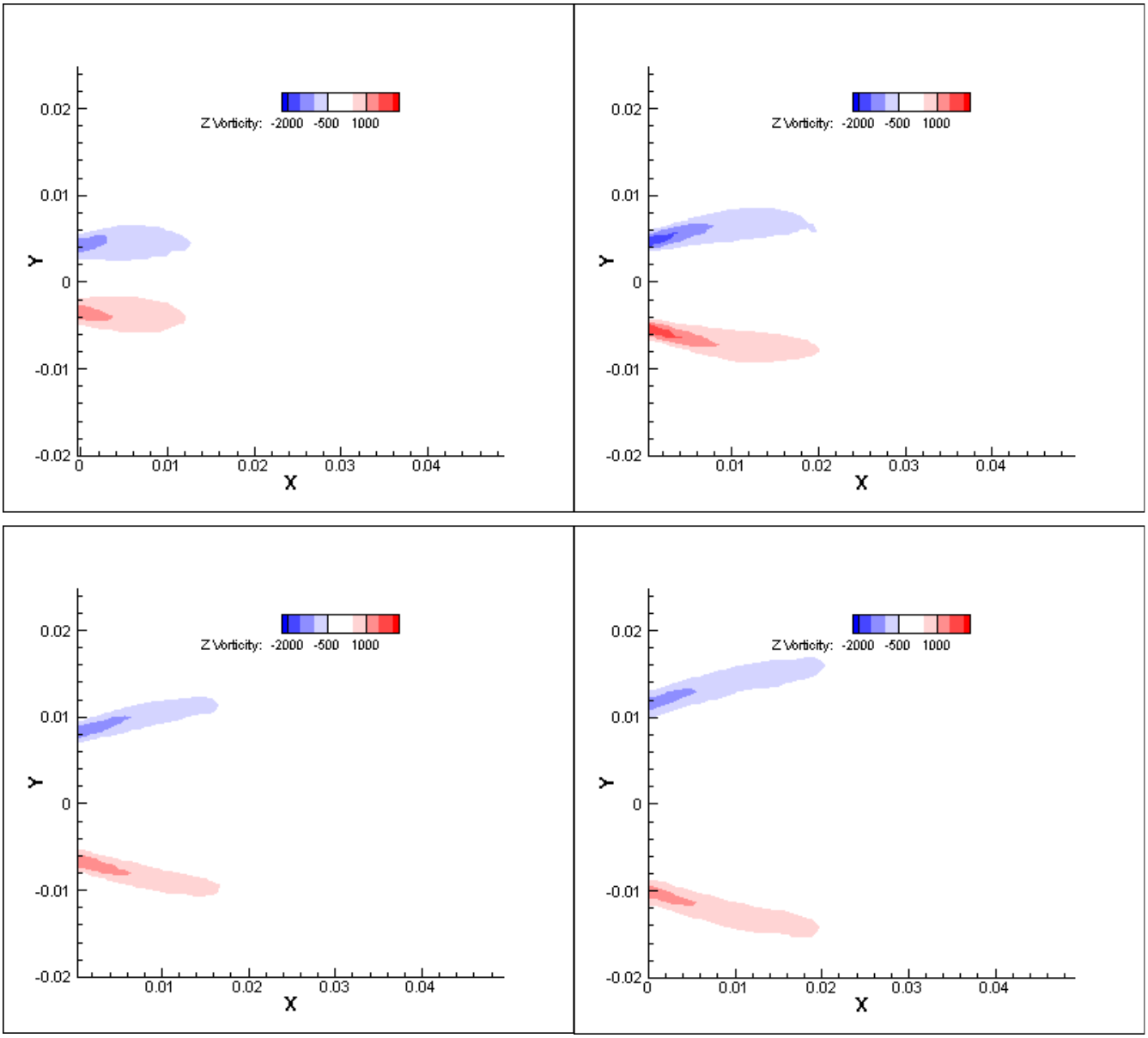

Figure 6: Top left: 6.35 mm triangular bluff body. Top right: 9.53 mm triangular bluff body. Bottom left: 12.7 mm triangular bluff body. Bottom right: 19.1 mm triangular bluff body. Axes are in units of meters and the flow direction is from left to right. The bluff body trailing edge is at x = -0.002 m and the centerline is along the y = 0 line. The flow is not acoustically excited.

Figure 7 shows the vorticity plots for the same bluff bodies as above but with an acoustically excited flow. Similar to the non-excited case (Figure 6), the divergence angle increases with bluff body size, although this is a smaller effect in the excited case. The vortex separation distance also increases with bluff body size. An interesting phenomenon is seen here that is not observed in the non-excited case: as the bluff body size is increased, the vortices become more concentrated and less spread out. However, the 19.1 mm bluff body does not follow this rule (Figure 7 bottom right). The overall vorticity field and the individual vortices actually decrease in strength; however, they remain more coherent further downstream as compared to the smaller bluff bodies.

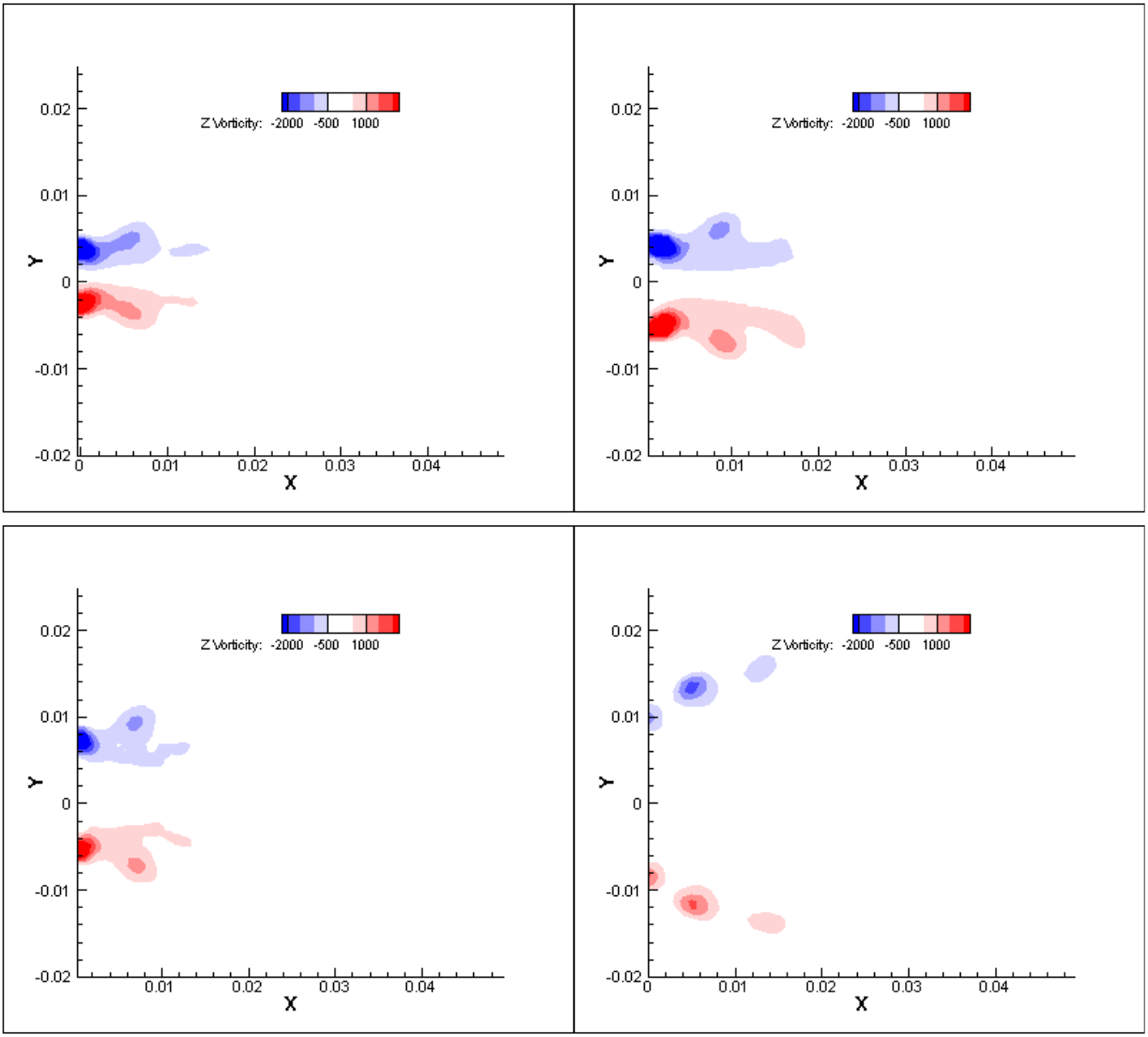

Figure 7: Top left: 6.35 mm triangular bluff body. Top right: 9.53 mm triangular bluff body. Bottom left: 12.7 mm triangular bluff body. Bottom right: 19.1 mm triangular bluff body. Axes are in units of meters and the flow direction is from left to right. The bluff body trailing edge is at x = -0.002 m and the centerline is along the y = 0 line. The flow is acoustically excited at 300 HZ, 180 degrees phase (with respect to the input acoustic signal) and $u'/U_\infty = 0.8$.

5.3. Effects of Heat Release

Heat release is another important factor that affects the flow dynamics in a major way. Figure 8 compares the effects of increased heat release (increased equivalence ratio, φ) for the non-excited flow. One observation is made from this comparison: the downstream vorticity reach initially increases with added heat release then decreases beyond $\varphi = 0.68$. The divergence angle does not change with heat release in a significant way and is concluded to be independent.

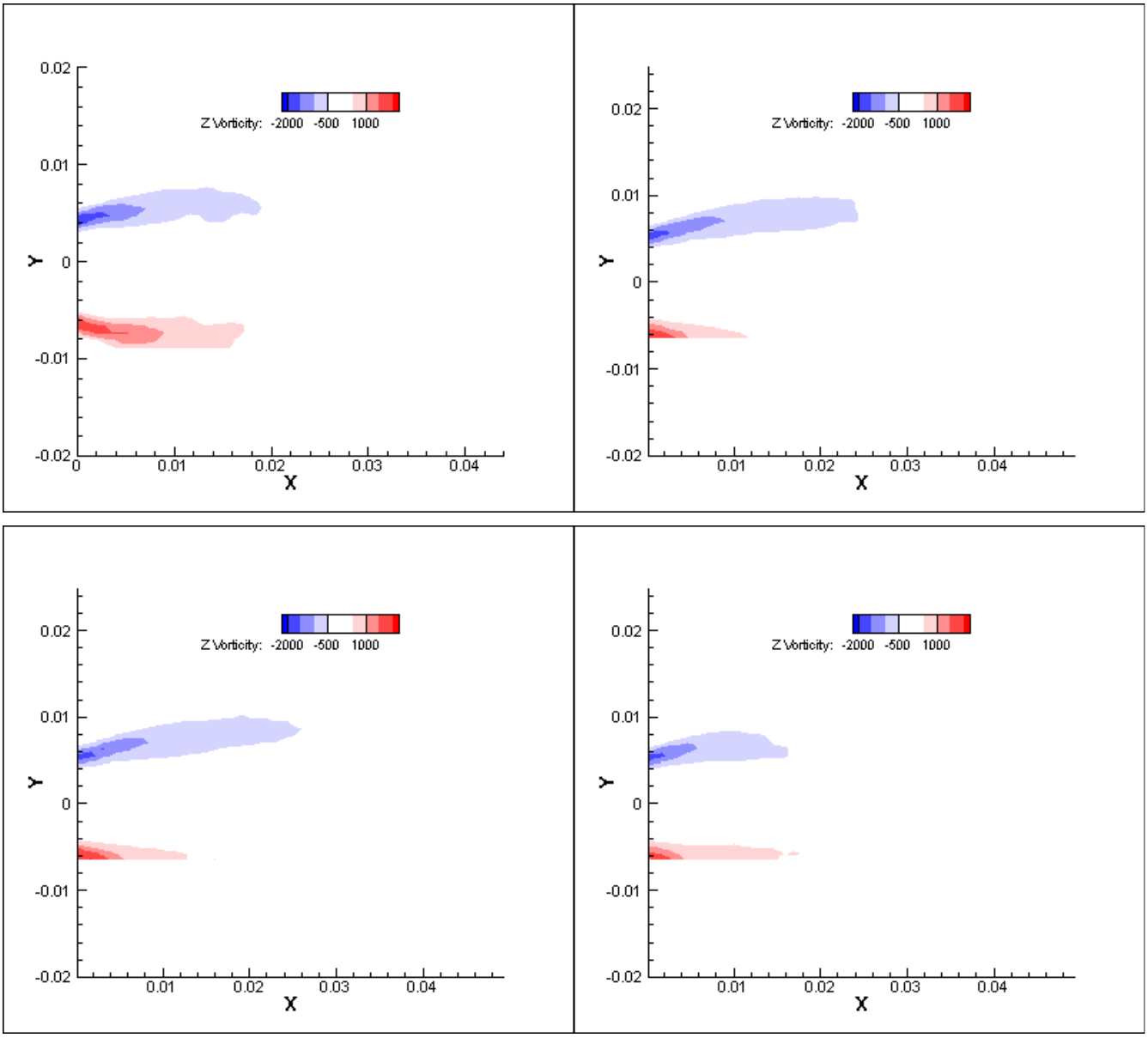

Figure 8: Top left: non-reacting flow, φ = 0. Top right: φ = 0.65. Bottom left: φ = 0.68. Bottom right: φ = 0.74. Axes are in units of meters and the flow direction is from left to right. The 9.53 mm triangular bluff body trailing edge is at x = -0.002 m, and the centerline is along the y = 0 line. The flow is not acoustically excited. In the latter three cases no data is recorded below y = -0.006 m.

The acoustically excited case produces more interesting results. Figure 9 shows the effects of heat release on the acoustically excited flow. From this figure, four key observations are made. First, the divergence angle increases from the non-reacting flow case (Figure 9 top left) to the reacting flow cases; however, the divergence angle does not change in the reacting flow if the equivalence ratio is

changed. Second, excluding the non-reacting flow case, Figure 9 suggests that downstream vorticity decays faster with increasing heat release. However, Figure 10 shows no coherent relationship between increasing heat release and downstream vorticity decay. Third, with increasing equivalence ratio, the net vorticity spreads out more and results in more colored area in the plots (this conclusion is only valid for this phase). Fourth, even though the divergence angle increases, the separation distance between vortices greatly decreases from the non-reacting flow to the reacting flow case. While increasing the equivalence ratio (and the heat release), the vortex boundaries get closer to each other as well.

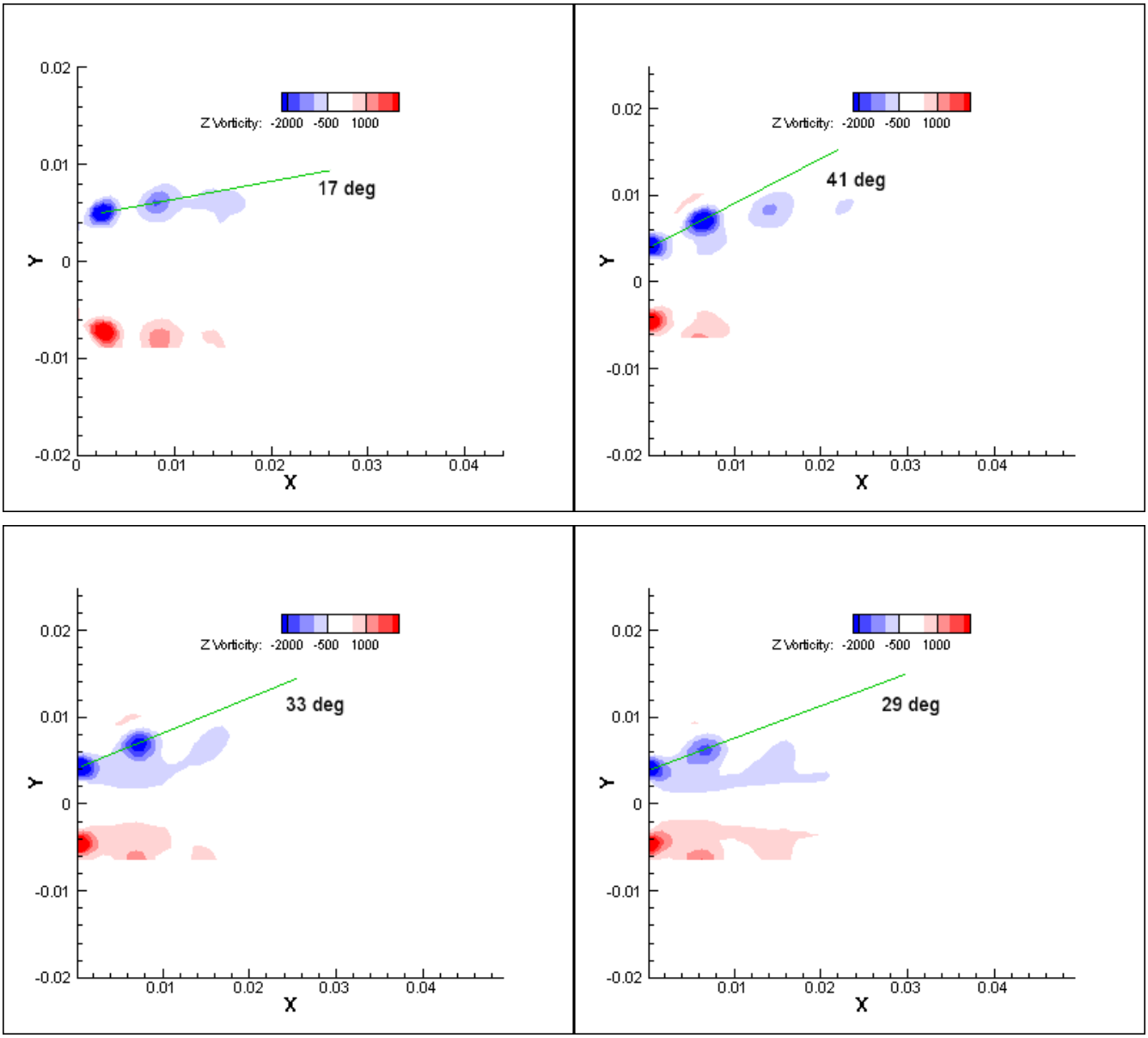

Figure 9: Top left: non-reacting flow, φ = 0. Top right: φ = 0.63. Bottom left: φ = 0.68. Bottom right: φ = 0.74. The green line represents the vorticity divergence angle with respect to the x-axis and the associated angle is labeled. Axes are in units of meters and the flow direction is from left to right. The 9.53 mm triangular bluff body trailing edge is at x = -0.002 m, and the centerline is along the y = 0 line. The flow is acoustically excited at 300 HZ, 135 degrees phase (with respect to the input acoustic signal) and $u'/U_\infty = 0.8$. *In the latter three cases no data is recorded below y = -0.006 m.*

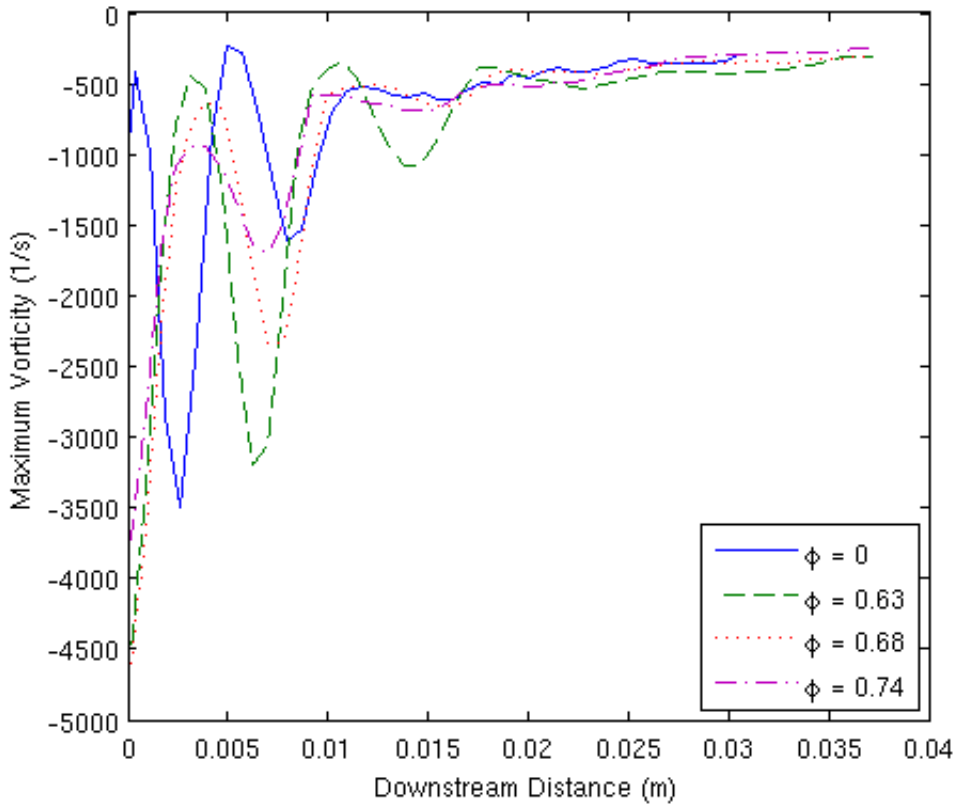

Figure 10: Plot of maximum vorticity along the downstream distance with four equivalence ratios. This data is generated from Figure 9. The flow direction is from left to right. The 9.53 mm triangular bluff body trailing edge is at x = -0.002 m, and the centerline is along the y = 0 line. The flow is acoustically excited at 300 HZ, 135 degrees phase (with respect to the input acoustic signal) and $u'/U_\infty = 0.8$.

6. Conclusions

Three key flow parameters are considered in this paper: vorticity divergence angle, downstream vorticity decay and vortex separation distance at the bluff body trailing edge. The effects of bluff body shape and size as well as heat release are examined in relation to the above mentioned parameters. The vorticity divergence angle is found to be affected by bluff body size and heat release but not affected by bluff body shape.

Downstream vorticity decay is affected by all three factors: 1) the triangular bluff body produces much stronger vortices and thus they propagate further downstream; 2) bluff body size and 3) heat release have a non-linear effect on vortex decay. Downstream vortex propagation is at a maximum for bluff body sizes above 6.35 mm and increases initially with added heat release, to reach a maximum at $\varphi = 0.68$ and then decrease.

Vortex separation distance is affected primarily by bluff body size. As bluff body size increases, the vortex separation distance increases monotonically. The vortex separation distance is also larger for the cylindrical bluff body when compared to the triangular bluff body; however this effect is only seen in the non-excited flow. Vortex separation distance decreases with increasing heat release.

7. Future Work

Several areas need to be researched further. To compare the trends of the triangular bluff body to the cylindrical bluff body a study must be done noting the effects of varying the cylindrical bluff body size. Another area of interest is chemiluminescence. This technique makes direct heat release measurements by relating specific reaction rates (typically of CH* and OH* radicals) to light emission at specific wavelengths [11]. Using a photomultiplier tube (PMT) and an optical filter, one is able to make direct heat release measurements and correlate them to acoustic oscillations (see a summary of these interaction processes).

However, to make this study more applicable, these experiments must be repeated at more realistic conditions. Typical flow velocities found in afterburners are 150 – 250 m/s while typical reactant temperatures are 650° – 1050° C [1]. A new experimental apparatus must be developed to test near these conditions.

8. References

[1] Lovett, J. A., Brogan, T. P., Philippona, D.S., Keil, B. V. and Thompson, T.V., "Development Needs for Advanced Afterburner Design", *40th AIAA/ASME/SAE/ASEE Joint Propulsion Conference*, Fort Lauderdale, FL, AIAA Paper 2004-4192, 2004

[2] Shanbhogue, S. J., Plaks, D. V., and Lieuwen, T., "The K-H Instability of Reacting, Acoustically Excited Bluff-Body Shear Layers", *43rd AIAA/ASME/SAE/ASEE Joint Propulsion Conference*, Cincinnati, OH, AIAA Paper 2007-5680, 2007.

[3] Prasad, A., and Williamson, C. H. K., "The Instability of the Shear Layer Separating from a Bluff Body", *J. Fluid Mech.*, Vol. 333, 1997, pp. 375-402

[4] Erickson, R. R., Soteriou, M. C., and Mehta, P. G., "The Influence of Temperature Ratio on the Dynamics of Bluff Body Stabilized Flames", *44th AIAA Aerospace Sciences Meeting*, Reno, NV, AIAA Paper 2006-753, 2006

[5] Mehta, P. G, and Soteriou, M. C., "Combustion Heat Release Effects on the Dynamics of Bluff Body Stabilized Premized Reacting Flows", *41st Aerospace Sciences Meeting*, Reno, NV, AIAA Paper 2003-835, 2003

[6] Shanbhogue, S. J., Plaks D. V., and Lieuwen, T., "Interaction of Bluff Body Flames with the Shear Layer under Harmonic Excitation", *21st International Colloquium on the Dynamics of Explosions and Reactive Systems (ICDERS)*, Poitiers, France, 2007

[7] Ducruix, S., Schuller, T., Durox, D., and Candel, S., "Combustion Dynamics and Instabilities: Elementary Coupling and Driving Mechanisms", *Journal of Propulsion and Power*, Vol. 19, No. 5, 2003, pp. 722-734

[8] Raffel, M., Willert, C., and Kompenhans, J., "Particle Image Velocimetry: A Practical Guide", Springer, 1998

[9] Turns, Stephen R., *An Introduction to Combustion: Concepts and Applications*. 2nd ed., McGraw-Hill Higher Education, Boston, 2000.

[10] Williams, F. A., "Flame Stabilization of Premixed Turbulent Gases," *Applied Mechanical Surveys* (N. N. Abramson, H. Liebowitz, J. M. Crowley, and S. Juhasz, eds.), Spartan Books, Washington DC, pp. 1157-1170, 1966.

[11] Muruganandam, T. M., Kim, B., Older, R., Patel, M., Romig, B., and Seitzman, J. M., "Chemiluminescence Based Sensors for Turbine Engines", *39th AIAA/ASME/SAE/ASEE Joint Propulsion Conference*, Huntsville, AL, AIAA Paper 2003-4490, 2003